Shear-Induced Molecular Orientation and Crystallization in Isotactic Polypropylene: Effects of the Deformation Rate and Strain

Rajesh H. Somani, Ling Yang, and Benjamin S. Hsiao*

Department of Chemistry, State University of New York, Stony Brook, New York 11794-3400

Thomas Sun

ExxonMobil Chemical Company, Baytown Polymers Center, Texas 77522

Natalia V. Pogodina and Arnold Lustiger

ExxonMobil Research and Engineering Company, Annandale, New Jersey 08801

Received August 20, 2004; Revised Manuscript Received November 22, 2004

ABSTRACT: Studies of dilute polymer solutions in shear flow suggest that the mean fractional extension of molecules increases gradually with the Weissenberg number (*Wi* = shear rate × longest relaxation time) and approaches an asymptotic value of 0.4−0.5, while in elongational flow it approaches full contour length above a certain critical strain rate. In an entangled polymer melt, this behavior is more complex due to inter- and intramolecular interactions. In situ rheo-SAXS (small-angle X-ray scattering) and -WAXD (wide-angle X-ray diffraction) experiments were performed to investigate the effects of shear rate, shear duration, and *Wi* on the extent of molecular orientation/extension and crystal orientation in an isotactic polypropylene (iPP) melt. Two series of experiments were designed: (1) variation of shear rate (30, 45, and 60 s^{-1}) at a constant shear duration (5 s) and (2) variation of shear duration (1.3, 3, and 5 s) at a constant rate (60 s^{-1}). The degree of crystal orientation (Herman's orientation function, *f*) observed at 165 °C and fraction of oriented crystals (X_o) observed in a fully crystallized sample at room temperature increased with both shear rate and shear duration. Interestingly, at a constant strain (rate × duration), short-duration shear at a high rate was found to be more effective (i.e., higher *f* and X_o) than long-duration shear at a low rate. The longest relaxation time for the iPP sample and *Wi* were estimated from the dynamic moduli data. Both *f* and X_o were found to gradually increase with *Wi* and approached plateau values at high values of *Wi*. Results indicated that, even under a very intense shear field (or high *Wi* values), molecules do not extend to full contour length, and there is a limiting value for mean orientation/extension and subsequent crystal orientation in a polymer matrix. Characteristic dimensions of the shish-kebab entity formed in a sheared iPP melt at 165 °C were determined from the rheo-SAXS data. It was found that the average shish length was 700−750 nm and the average spacing between adjacent kebabs was 60−70 nm.

Introduction

In most processing operations, polymer melts are subjected to flow prior to crystallization. The crystallization behavior and resultant morphology are dictated by the applied flow conditions, such as temperature, deformation strain, and deformation rate.[1−16] In general, crystallization follows two-step processes involving nucleation and growth. Previous studies have shown that, under flow, tiny primary nuclei are generated at very early stages of crystallization. The process of nuclei formation can be extremely fast, on the order of nanoseconds.[17] The nature of first formed primary nuclei and their spatial arrangement and correlations (i.e., their landscape) essentially dictate the subsequent crystal growth and morphological development. Therefore, to control the polymer morphology, understanding the inter- and intramolecular interactions in flow is essential. This subject has drawn the considerable interest of many research groups in the past, such as Keller et al.,[18−24] Janeschitz-Kriegl et al.,[25−28] Winter et al.,[29−32] Kornfield et al.,[33−36] Strobl et al.,[37−39] Lotz et al.,[40−42] Mitchell et al.,[43,44] de Jeu et al.,[45,46] Monasse et al.,[47−49] Ryan et al.,[50−53] Muthukumar et al.,[54−57] Alfonso et al.,[58−61] Frenkel et al.,[62] and many others.

* To whom correspondence should be addressed. Phone: (631) 632-7793. Fax: (631) 632-6518. E-mail: bhsiao@notes.cc.sunysb.edu.

The imposed flow intensity will affect molecular configuration, and its ability to organize, align, and form primary nuclei. The shear process can be characterized by the Weissenberg number, *Wi*, which is the ratio between the flow time scale (reciprocal shear rate) and the diffusion time scale (the longest relaxation time), accounting for Brownian motion-induced configuration changes. S. Chu et al.[63−67] have reported elegant studies of the conformational dynamics of individual, flexible polymers (labeled DNA molecules) in dilute solutions under flow by video fluorescence microscopy. In steady-state shear, the mean fractional extension was found to increase gradually with *Wi* and approach an asymptotic value of 0.4−0.5. This behavior differs markedly from that in pure elongational flow, where molecular extension increases rapidly to a value close to the full contour length of the chain at relatively low deformation rates. The corresponding situation in an entangled melt is more complex due to inter- and intramolecular interactions. Intuitively, polymer chain dynamics is expected to be affected by the characteristics of the surrounding matrix, such as viscosity, mesh size, or molecular weight between the entanglements. How these affect the events in polymer crystallization and subsequent morphology or microstructure, i.e., the nature and the distribution of the oriented and unoriented fractions in the crystalline phase, is still not clear.

10.1021/ma048285d CCC: $30.25
Published on Web 01/22/2005

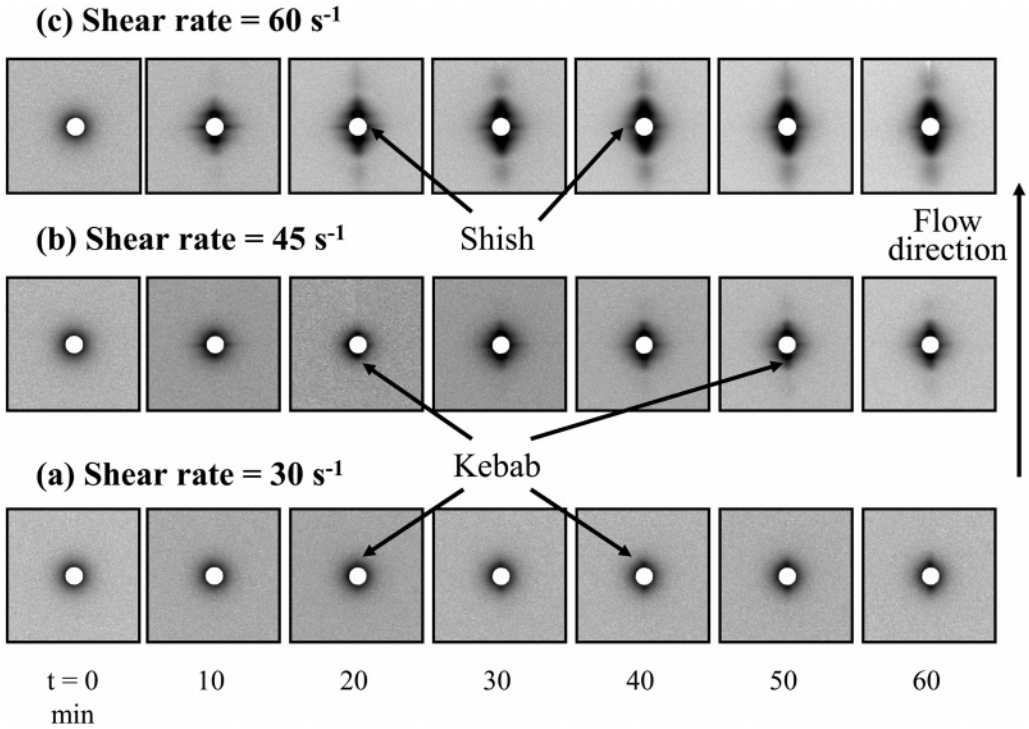

Figure 1. 2D SAXS images of the iPP melt at selected times after shear at different shear rates: (a) 30 s^{-1}, (b) 45 s^{-1}, and (c) 60 s^{-1} (shear duration 5 s and T = 165 °C).

Over the past several years, our group has focused our research efforts on understanding the nature of initially formed nuclei in sheared polymer melts.[68−78] The various polymer systems investigated include isotactic polypropylene (iPP) at 165 °C,[69−72] iPP at 140−150 °C,[73−75] long-chain branched iPP,[76] a blend of iPP and atactic PP,[77] and low and high molecular weight polyethylenes and their blends.[78] In this paper, we extend the previous studies and probe the effects of shear rate, shear duration, and *Wi* on the extent of molecular orientation/extension, oriented crystal development, and final microstructure in iPP.

Experimental Section

A Ziegler−Natta iPP homopolymer, supplied by ExxonMobil Chemical Co., was used in the present experiments. Its molecular weights were M_n = 92000, M_w = 368000, and M_z = 965000. The details of the Linkam shear apparatus and synchrotron X-ray experimental procedures have been described in our previous publications.[69−71] Briefly, the temperature protocol for shear experiments was as follows: (1) Heat the polymer sample from room temperature to 200 °C at a rate of 30 °C/min. (2) Hold the temperature at 200 °C for 5 min. (3) Cool the sample at a rate of 30 °C/min to 165 °C. (4) Hold the temperature at 165 °C for 60 min; X-ray images were collected continuously during this period under deformation. (5) Cool the sample to room temperature at 10 °C/min; one X-ray pattern was collected at room temperature after crystallization of the sheared melt.

In situ rheo-SAXS (small-angle X-ray scattering) and -WAXD (wide-angle X-ray diffraction) measurements were carried out in the X3A2 beamline at the National Synchrotron Light Source (NSLS), Brookhaven National Laboratory (BNL). A 2D MAR-CCD X-ray detector (MARUSA) having a resolution of 1024 × 1024 pixels (pixel size 158 μm) was employed to collect time-resolved SAXS and WAXD patterns. The sample-to-detector distances for SAXS and WAXD experiments were 1600 and 107.4 mm, respectively. One X-ray pattern of the amorphous, isotropic melt was collected immediately when the temperature reached 165 °C prior to shear. Subsequently, the polymer melt was subjected to the following shear conditions: Three shear rates, 30, 45, and 60 s^{-1}, at a constant duration of 5 s, and three shear durations, 1.3, 3, and 5 s, at a constant shear rate of 60 s^{-1}, were chosen for the shear experiments. Two-dimensional patterns (SAXS or WAXD) were collected continuously, before, during, and after cessation of shear. In addition, one X-ray pattern was collected after the sample was cooled to room temperature. All X-ray data were corrected for background scattering before analysis.

The shear field was applied by rotating the bottom plate of the Linkam shear stage at an angular velocity, ω (corresponding to the desired shear rate = $r\omega/d$, with d being the sample thickness or the gap between the two plates and r being the radius), for the desired duration of time, while the top plate remained stationary. Thus, the velocity was maximum at the surface of the rotating plate and zero at the surface of the stationary plate. The resultant velocity gradient was linear or constant across the sample thickness, and therefore, the shear rate at any point in the gap was also constant. The total strain or the degree of molecular orientation, however, was maximum at the surface of the rotating plate and zero at the surface of the stationary plate. Hence, the molecular orientation profile in the gap was linear, corresponding to the velocity profile. The X-ray patterns represented the average of the oriented structures in the bulk of the sample across its thickness.

Results

Rheo-SAXS. (a) In Situ SAXS Images under Different Shear Conditions. 2D SAXS patterns at selected times after shear at shear rates of 30, 45, and 60 s^{-1} are presented in parts a−c of Figure 1, respectively. A constant shear duration of 5 s was used in these experiments. The flow direction is vertical, and it is considered the same as the fiber axis (we assume the deformed scatterers have a fiber symmetry). All SAXS images before shear (at t = 0) showed diffused scattering from the isotropic melt, indicative of noncrystalline structures without preferred orientation. Typically, the appearance of a relatively weak equatorial streak in SAXS patterns can be attributed to the shish-like crystalline/mesomorphic structure, oriented parallel to

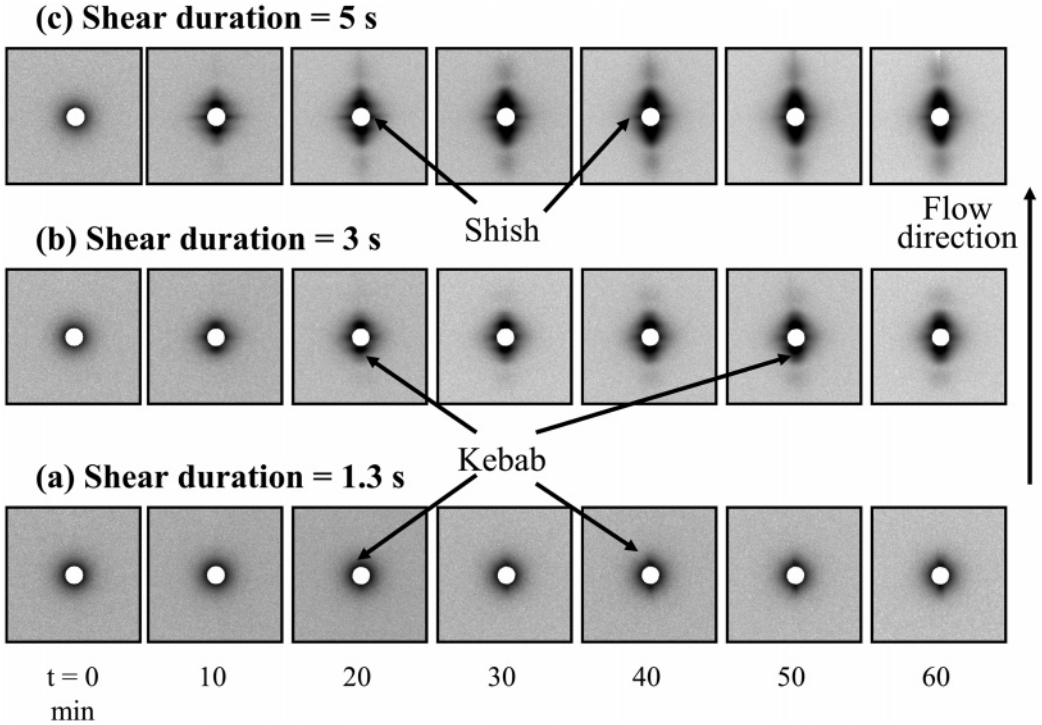

Figure 2. 2D SAXS images of the iPP melt at selected times after shear at different shear durations: (a) 1.3 s, (b) 3 s, and (c) 5 s (shear rate 60 s^{-1} and $T = 165$ °C).

the flow direction, while the appearance of strong meridional maxima can be attributed to kebab-like lamellar stacks, oriented perpendicularly to the flow direction.[69] However, in Figure 1a, the SAXS images at a shear rate of 30 s^{-1} showed no sign of equatorial streak, but only weak meridional maxima, while at shear rates of 45 and 60 s^{-1}, both strong equatorial streaks and meridional maxima were observed, indicative of the formation of shish-kebab morphology in the melt. The absence of the equatorial streak at low shear rate (30 s^{-1}) does not necessarily mean that the shish did not form; it is more likely that the size of the shishes is simply too small and/or the volume fraction of the shish is too low to induce a detectable SAXS signal. The observed meridional maxima are caused by crystalline lamellae initiated from the small shish since these maxima do not form in the absence of shear. At high shear rates (45 and 60 s^{-1}), the equatorial streaks observed in SAXS are a direct indicator of the shish formation in the melt. The equatorial streaks appeared immediately after the imposed shear, suggesting that orientation/extension of polymer molecules is high under these conditions. The strong meridional maxima observed in these patterns are indicative of the large volume fraction of the shish. These patterns show that the SAXS intensity and therefore the amount of shear-induced oriented crystals in the polymer melt increase with shear rate (at a constant shear duration).

Parts a−c of Figure 2 exhibit 2D SAXS images at selected times after the melt was subjected to shear durations, t_s, of 1.3, 3, and 5 s, respectively. A constant shear rate of 60 s^{-1} was used in these experiments. The SAXS patterns in Figure 2 are similar to the patterns in Figure 1. At a shear duration of 1.3 s, only meridional maxima were observed, while at shear durations of 3 and 5 s, both equatorial streaks and meridional maxima were detected. As discussed above, the equatorial streak could not be observed at shorter shear duration probably because of the small size of the shish and/or the small volume fraction of the shish. On the other hand, at longer shear duration, orientation/extension of molecules is high, and therefore, the size of the shish becomes sufficiently large and/or the volume fraction of the shish becomes sufficiently high to result in distinctive equatorial streaks in the corresponding SAXS patterns. In addition, strong meridional maxima were observed in these patterns, which is indicative of a high volume fraction of kebabs. It is seen that the SAXS intensity and thus quantity of the shear-induced oriented crystals increase with shear duration (at a constant shear rate).

Visual comparison of SAXS patterns in Figures 1 and 2 shows the differences, qualitatively, in the nature of shear-induced oriented crystals under different shear conditions. As one might expect, the SAXS intensity increases with shear rate (at constant shear duration) as well as with shear duration (at constant shear rate). Interestingly, it is seen in these patterns that, at a constant strain, there are significant differences in the effects of short-duration shear at a high shear rate versus long-duration shear at a low shear rate. For example, comparison of the patterns in Figures 1a and 2a reveals that the SAXS intensity at a shear rate of 60 s^{-1} and $t_s = 1.3$ s (strain 78) is stronger than that at a shear rate of 30 s^{-1} and $t_s = 5$ s (strain 150). Similarly, comparison of the patterns in Figure 2b versus Figure 1b shows that the intensity is stronger at a shear rate of 60 s^{-1} and $t_s = 3$ s (strain 180) than that at 45 s^{-1} and $t_s = 5$ s (strain 225). Thus, we conclude that, at a constant strain, the degree of crystal orientation and oriented crystal fraction are higher in short-duration shear at a high shear rate than those in long-duration shear at a low shear rate.

(b) Ex Situ SAXS Images after Cooling. Figure 3 shows SAXS patterns of the crystallized iPP obtained after cooling of the sheared melt to room temperature (note that the melt was cooled at the end of the

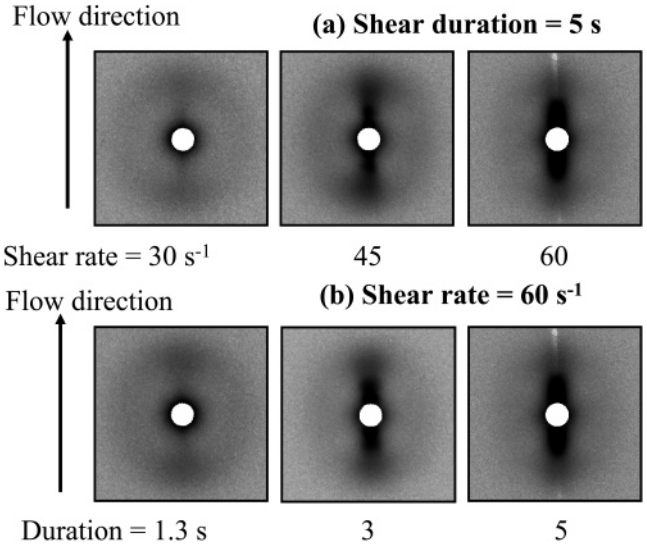

Figure 3. 2D SAXS images of a sheared iPP polymer at room temperature: (a) at different shear rates (constant shear duration 5 s), (b) at different shear durations (constant shear rate 60 s^{-1}). Note that the sheared melt was kept at 165 °C for 1 h after cessation of shear, and then cooled to room temperature.

isothermal rheo-SAXS/WAXD experiment; i.e., 1 h after shear). The SAXS images at different shear rates (at constant t_s) are shown in Figure 3a, and those at different shear durations (constant shear rate) are shown in Figure 3b. Before cooling, the sheared melt at 165 °C primarily consists of high-temperature stable oriented crystals, as seen in the corresponding SAXS patterns. In these patterns there is no evidence of scattering due to unoriented crystals. Upon cooling, obviously, all crystallizable species in the melt would crystallize. It is expected that while new unoriented crystals will simultaneously nucleate and grow, the first formed oriented crystals will also grow with the same preferential orientation. The overlap of diffused scattering due to the unoriented crystals and scattering due to the oriented crystals is clearly seen in the SAXS patterns in Figure 3. It should be noted that the increase in the scattering intensity along the meridian is due to the following factors: (1) growth of previously formed oriented crystals, (2) perfection of previously formed oriented crystals (i.e., it is expected that during cooling there is reorganization of the chain segments within lamellae, which increases electron density contrast), and (3) nucleation and growth of the unoriented crystals. Figure 3 is visual evidence of the significant effects of shear intensity (rate and duration) on the morphology and microstructure of the completely crystallized polymer.

Rheo-WAXD. At a wavelength of 1.54 Å, the monoclinic α-crystalline form of iPP reflections can be indexed as follows in the WAXD profile:[75] (110) at $2\theta = 14.1°$, (040) at 16.9°, (130) at 18.5°, (111) at 21.4°, and (−131) at 21.8°. In 2D WAXD patterns, crystal orientation can further be determined from the azimuthal variation in the intensity of the appropriate crystal reflections. When the crystal orientation is high, the azimuthal breadths are relatively narrow, leading to the appearance of arclike or pointlike diffraction features. On the other hand, the crystals without preferred orientation exhibit circular rings of uniform intensity.

(a) In Situ WAXD Images under Different Shear Conditions. 2D WAXD patterns at selected times after shear at shear rates of 30, 45, and 60 s^{-1} (at a constant shear duration), corresponding to the SAXS patterns in Figure 1, are shown in parts a−c of Figure 4, respectively. At a shear rate of 30 s^{-1}, no crystal reflections were detected, even 1 h after shear. However, the corresponding SAXS patterns in Figure 1 show distinct meridional maxima. This result is due to the fact that the detection limit of WAXD is about 1 order of magnitude poorer than that of SAXS.[68,69] Since the volume fraction of the formed crystals is expected to be relatively low at 165 °C under low shear rates, its

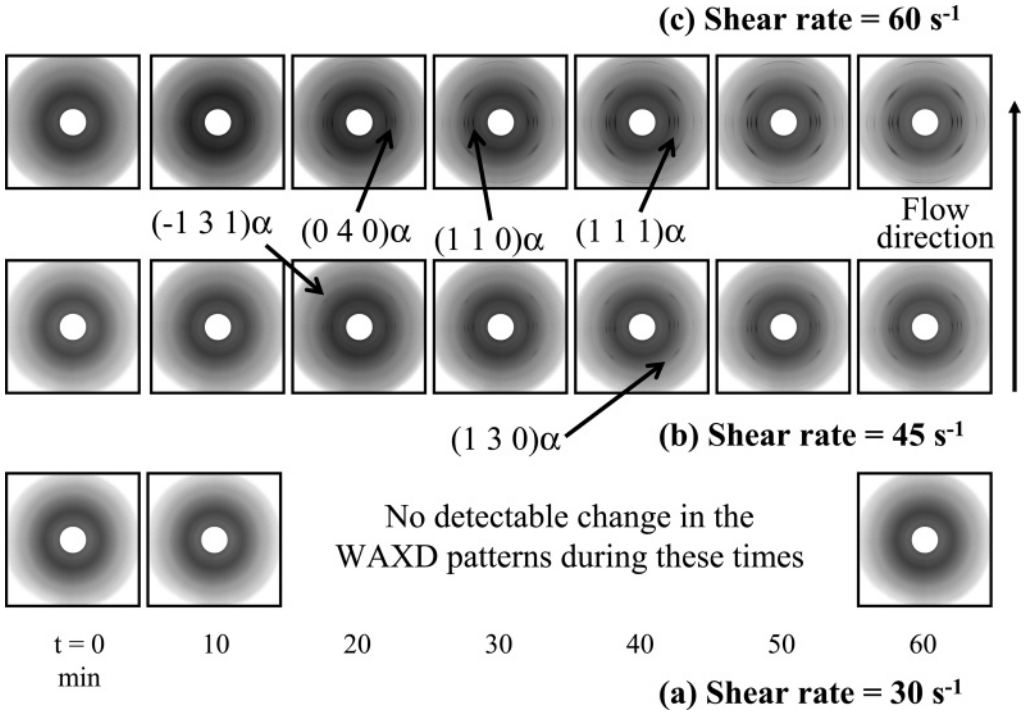

Figure 4. 2D WAXD images of the iPP melt at selected times after shear at different shear rates: (a) 30 s^{-1}, (b) 45 s^{-1}, and (c) 60 s^{-1} (shear duration 5 s and $T = 165$ °C).

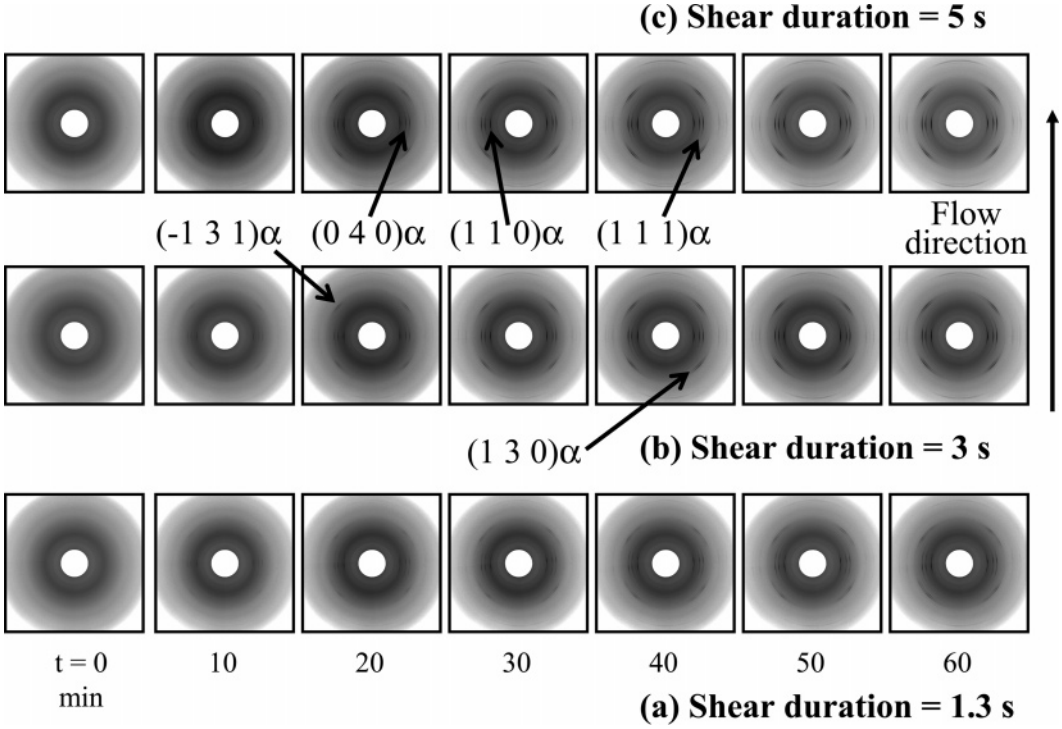

Figure 5. 2D WAXD images of the iPP melt at selected times after shear at different shear durations: (a) 1.3 s, (b) 3 s, and (c) 5 s (shear rate 60 s^{-1} and $T = 165$ °C).

crystal reflections could not be resolved by WAXD. On the other hand, due to the higher nucleation density the quantity of crystals formed is high at high shear rates (45 and 60 s^{-1}); therefore, crystal reflections are strong and detectable in WAXD. Variation in the intensity of crystal reflections as a function of time can be clearly seen in these patterns. Note that the azimuthal breadths in the intensity of the reflections are relatively narrow, indicative of high crystal orientation. As expected, the degree of orientation increases with shear rate (at a constant shear duration), which is consistent with the corresponding SAXS observations in Figure 1.

Parts a−c of Figure 5 show 2D WAXD patterns at selected times after shear at shear durations of 1.3, 3, and 5 s (and at a constant shear rate), respectively, corresponding to the SAXS patterns in Figure 2. Similar to Figure 4, the azimuthal breadths in the intensity of the reflections are also narrow, indicative of strong crystal orientation. The variation in the intensity of crystal reflections with time is clearly seen in these patterns. As expected, the degree of crystal orientation increases with shear duration (at a constant shear rate), consistent with the corresponding SAXS observations in Figure 2.

(b) Ex Situ WAXD Images after Cooling. Figures 6a and 7a show 2D WAXD patterns of the crystallized iPP obtained after cooling of the sheared melt to room temperature. Figure 6a shows the patterns obtained at shear rates of 30, 45, and 60 s^{-1}. Figure 7a shows the patterns at shear durations of 1.3, 3, and 5 s. The corresponding 3D profiles are shown in Figures 6b and 7b. As mentioned above, the sheared melt at 165 °C primarily consists of high-temperature stable oriented crystals. Upon cooling, the first formed oriented crystals grow as well as become more perfect (realignment of chain segments), while new oriented and unoriented crystals can also simultaneously nucleate and grow. The effects of the imposed shear intensity (shear rate and shear duration) on the amount and degree of orientation

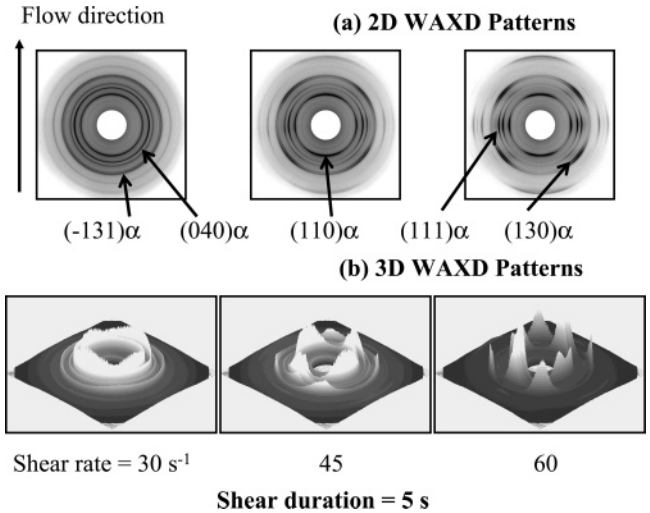

Figure 6. (a) 2D and (b) 3D WAXD patterns of the sheared iPP polymer at room temperature. Note that the sheared melt was kept at 165 °C for 1 h after cessation of shear and then cooled to room temperature (shear duration 5 s).

of the oriented crystals are clearly seen in the 3D profiles. Figures 6 and 7 confirm the observation in the rheo-SAXS experiments that, at a constant total strain, the degree of crystal orientation and oriented crystal fraction are higher in short-duration shear at a high shear rate than those in long-duration shear at a low shear rate.

Analysis of Rheo-SAXS and -WAXD Data. (a) Long Period from SAXS. The long period or the average spacing between the adjacent lamellae in kebabs was calculated from the Lorentz-corrected 1D SAXS intensity profiles (Iq^2 versus q, $q = (4\pi/\lambda) \sin \theta$, where λ is the wavelength of the X-ray beam and θ is half of the scattering angle) along the meridian of SAXS patterns. Parts a and b of Figure 8 compare the meridional intensity profiles at different shear rates and

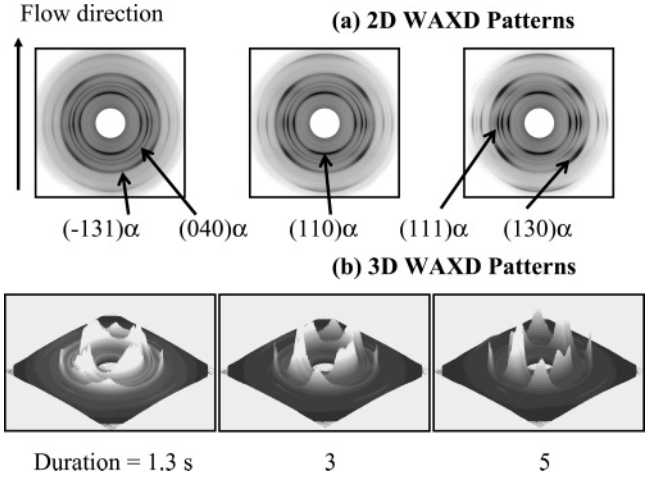

Figure 7. (a) 2D and (b) 3D WAXD patterns of the sheared iPP polymer at room temperature. Note that the sheared melt was kept at 165 °C for 1 h after cessation of shear and then cooled to room temperature (shear rate 60 s^{-1}).

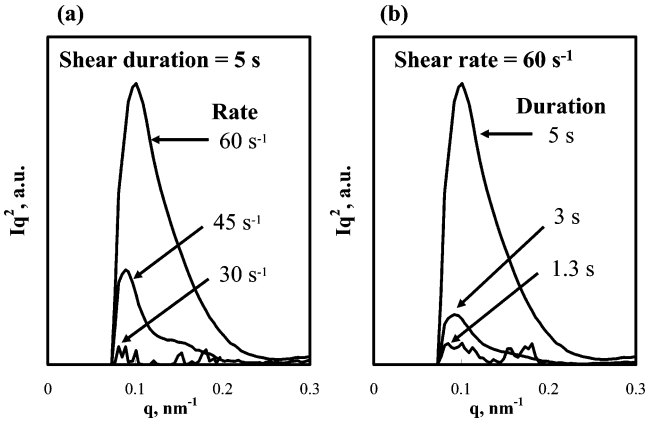

Figure 8. Lorentz-corrected SAXS intensity profiles taken along the meridian 1 h after shear (T = 165 °C): (a) at different shear rates (constant shear duration), (b) at different shear durations (constant shear rate).

durations, respectively. At weak shear conditions (i.e., a shear rate of 30 s^{-1} in Figure 8a and t_s = 1.3 s in Figure 8b), the scattering signal is low due to the low concentration of crystals. Hence, the signal/noise ratio is low, and the position of the scattering peak (q_{max}) in the meridional intensity profile could not be determined with high precision. However, at strong shear conditions, the signal is strong, the peak position could be accurately measured, and precise values of the long period were determined. At all the shear conditions, the long period of the kebabs ($L = 2\pi/q_{max}$) was found to be between 60 and 70 nm. Typically, the long period in quiescently crystallized semicrystalline iPP at room temperature is in the range of 20−30 nm.[79] The large long period is an indication of loosely packed, lamellae stacks. Interestingly, the long period value does not change with either shear rate or shear duration. This is because the extent of supercooling below the equilibrium temperature, $\Delta T = T_m^0 - T$ is probably the most dominating factor that controls the lamellae thickness and the corresponding long period. Since all experiments were performed at a constant temperature of 165 °C, the lamellae long period is more or less the same.

(b) Estimate of the Shish Length. To characterize the shish structure observed in rheo-SAXS patterns, a method demonstrated by Ruland[80] was used to analyze the intensity distribution of the equatorial streak. The

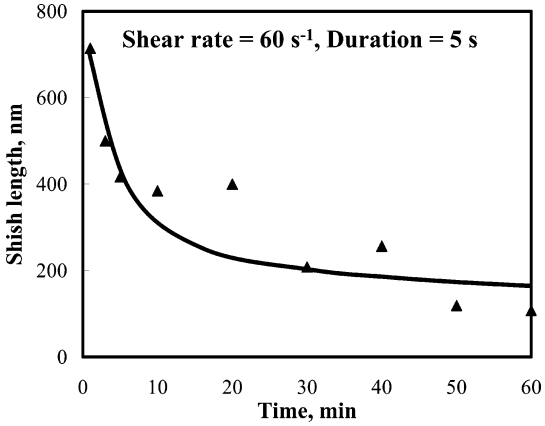

Figure 9. Length of the shish as a function of time after shear (shear rate 60 s^{-1}, shear duration 5 s, and T = 165 °C).

length of the streak along the equator in reciprocal space corresponds to the inverse diameter ($1/D$) of the shish in real space; the width of the streak in reciprocal space corresponds to the inverse length ($1/l_f$) of the shish. In this method, a series of azimuthal scans at different values of scattering vector **s** ($=q/2\pi$) along the equator are performed and fitted with a function, such as Lorentzian or Gaussian (the Lorentzian function gave a better fit than the Gaussian function in the present case). The integral breadth, B_{obs} (peak area/peak height), of each azimuthal profile is then determined as a function of **s**. The relationship between the shish length and its misorientation width, B_ϕ, can be given by the following equation:[80]

$$B_{obs} = \frac{1}{l_f}\frac{1}{\mathbf{s}} + B_\phi \qquad (1)$$

Thus, l_f can be obtained from the slope of B_{obs} versus $1/\mathbf{s}$ plot, and the intercept gives the misorientation width.

We note that, as the intensity along the equator was rather weak due to the high temperature of the experiment (since the corresponding crystallinity was low), the relationship between B_{obs} and $1/\mathbf{s}$ with good statistical significance could only be established in SAXS patterns collected at a shear rate of 60 s^{-1} and t_s = 5 s. Results of the estimated shish length as a function of time are shown in Figure 9. The shish length was about 700 nm immediately after shear; it decreased to about 150 nm at the end of the experiment (t = 60 min). Intuitively, one may have expected the shish to grow with time in the same way that the kebabs grow under the same conditions. The opposite trend is observed in Figure 9, indicating that the shish is "shrinking" or its average length is decreasing with time after shear. This anomaly requires some explanation. It should be noted that the growth of kebabs that are oriented perpendicular to the shish axis is very rapid, as seen in the SAXS patterns in Figures 1−3. It is our opinion that the development of kebabs may have imposed spatial-dependent local stress, which tends to relax orientation at several discrete points along the shish length, thus "shortening" the overall projection length of the shish-kebab entity. Its true length is probably preserved, although relaxation of chain ends and some loss in the average degree of orientation are possible after cessation of shear. We found that these analyses are consistent with our observations in polyethylene blend systems.[78] In con-

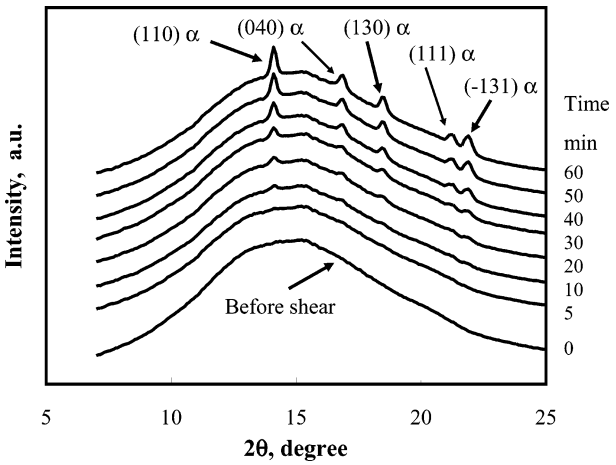

Figure 10. Circularly averaged WAXD intensity profiles at selected times after shear (shear rate 45 s^{-1}, shear duration 5 s, and T = 165 °C).

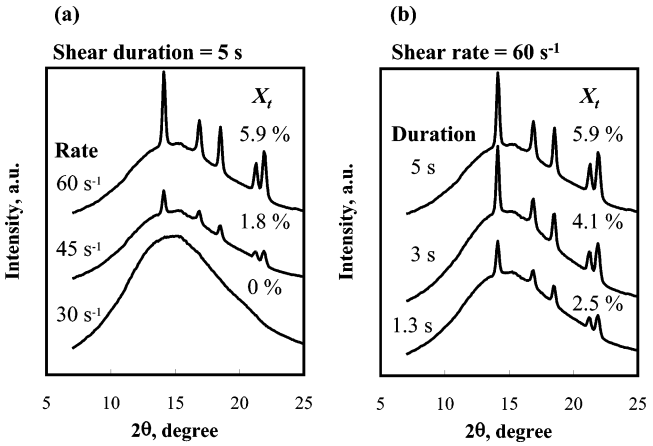

Figure 11. Circularly averaged WAXD profiles 1 h after shear (T = 165 °C): (a) at different shear rates (constant shear duration), (b) at different shear durations (constant shear rate). X_t represents the total crystallinity.

trast, the kebabs are found to grow with time because they are not dependent on the chain orientation; they simply grow in register with the previously formed chain-folded lamellae which comprise the kebabs. We estimate the shish length to be in the range of 700−750 nm and the long spacing of the kebab to be in the range of 60−70 nm. The long length of the shish indicates that chains in the shish probably traverse several nuclei from which kebabs originate, consistent with the simulation results of Muthukumar et al.[57] Our results allowed a quantitative estimate of the dimensions of the shish-kebab entity in the iPP melt under shear.

(c) WAXD Crystallinity Development at High Temperature. The amount of total crystalline phase was estimated from circularly averaged WAXD intensity profiles. To illustrate the calculation procedure, the averaged WAXD intensity profiles at selected times after cessation of shear (shear rate 45 s^{-1}, t_s = 5 s) are shown in Figure 10. A standard peak-fitting routine, described elsewhere,[75] was used to deconvolute the peaks in WAXD profiles. The normalized integrated intensity (peak area) of each crystal reflection and that of the amorphous background were obtained from the above fitting. The percent total crystalline phase (we termed the crystallinity index) in the polymer melt was calculated after subtraction of the area of the amorphous background. Note that the calculation of the crystallinity index by the above procedure is prone to error, especially when the WAXD pattern has strong peaks near the meridian, where a "Fraser correction" procedure[81] is normally utilized to correct for the missing diffraction intensity. In the present case, since most of the crystal reflections show strong peaks along the equator, it is our opinion that the crystallinity index estimated from the above analysis is probably close to the true crystallinity (we thus term the crystallinity index as crystallinity, X_t, hereafter), and results are useful for comparison of the volume fraction of oriented crystals formed under varying shear conditions. The average WAXD intensity profiles 1 h after shear at different shear rates and durations are shown in parts a and b of Figure 11, respectively. Note that the crystal reflections could not be resolved in the profile at a shear rate of 30 s^{-1}, due to the low volume fraction of the crystals. As expected, parts a and b of Figure 11 show that the intensity of the crystal reflections increases with shear rate as well as with shear duration, consistent with the corresponding SAXS observations. The calculated values of crystallinity at various shear conditions are also shown in Figure 11. It is seen that even 1 h after shear the obtained crystallinity values are generally low. This is because at 165 °C only oriented crystals with a higher melting point can survive. Thus, the value of X_t at 165 °C represents the amount of oriented crystals ($X_o = X_t$) and is directly dependent upon the extent of molecular orientation/extension induced by the imposed shear flow. In Figure 11, it is seen that X_t = 2.5% at a shear rate of 60 s^{-1} and t_s = 1.3 s (strain 78) compared to $X_t \approx 0\%$ at a shear rate of 30 s^{-1} and t_s = 5 s (strain 150). Also, X_t = 4.1% at a shear rate of 60 s^{-1} and t_s = 3 s (strain 180) compared to X_t = 1.8% at a shear rate of 45 s^{-1} and t_s = 5 s (strain 225). These results are in agreement with the qualitative trend observed in the SAXS images in Figures 1 and 2. Even when the strain is lower, the amount of oriented crystals is higher in short-duration shear at a high shear rate than that in long-duration shear at a low shear rate. This is a manifestation of a more pronounced effect of short-duration shear at a high shear rate on the molecular orientation/extension compared to that of long-duration shear at a low shear rate.

(d) Degree of Crystal Orientation at High Temperatures. Herman's method[82] was used to determine the degree of orientation of lamellae crystals in the sheared melt. Accordingly, the crystalline orientation can be characterized by the average orientation of the normal to the crystalline plane with respect to an external reference frame. Here, the flow direction was taken as the reference direction. For a set of *hkl* planes, the average orientation, expressed as $\langle \cos^2 \phi \rangle_{hkl}$, can be calculated mathematically using the following equation:[82]

$$\langle \cos^2 \phi \rangle_{hkl} = \frac{\int_0^{\pi/2} I(\phi) \cos^2 \phi \sin \phi \, d\phi}{\int_0^{\pi/2} I(\phi) \sin \phi \, d\phi} \qquad (2)$$

where ϕ is the azimuthal angle and $I(\phi)$ is the scattered intensity along the angle ϕ. Herman's orientation function, f, can be defined as

$$f = \frac{3\langle \cos^2 \phi \rangle_{hkl} - 1}{2} \qquad (3)$$

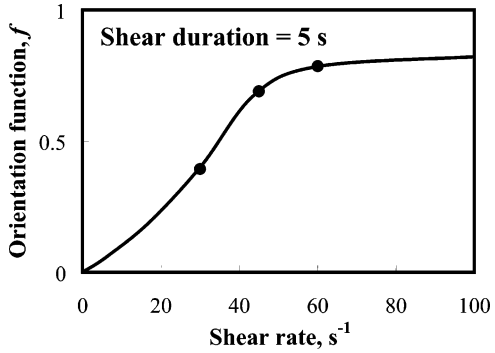

Figure 12. Herman's orientation function, f, 1 h after shear as a function of shear rate (shear duration 5 s and $T = 165$ °C).

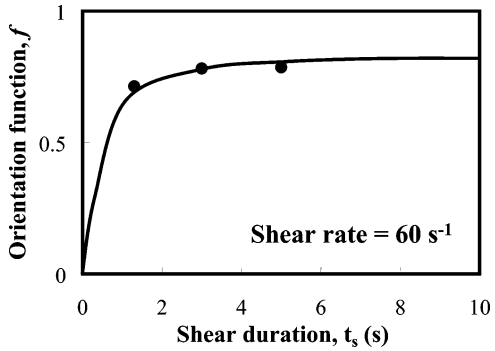

Figure 13. Herman's orientation function, f, 1 h after shear as a function of shear duration (shear rate 60 s^{-1} and $T = 165$ °C).

where f has a value of -0.5 when the normal of the reflection plane is perpendicular to the reference direction ($\phi = 90°$ or crystals are oriented parallel to the flow direction), a value of 1 when the normal is parallel to the reference direction ($\phi = 0°$ or crystals are oriented perpendicular to the flow direction), and a value of 0 when the orientation is random. For evaluation of the degree of orientation, the azimuthal intensity distribution $I(\phi)$ at $2\theta = 14.1°$ was analyzed. This peak represents the (110) reflection of α-crystals in iPP, which appears at the equator in the WAXD patterns.

Figures 12 and 13 show the value f (at $t = 60$ min after shear) as a function of shear rate and shear duration, respectively. It is interesting to note that the calculated f value is finite at a shear rate of 30 s^{-1}, even though crystal reflections could not be resolved in the WAXD pattern (Figure 4c). This can be explained as follows. The corresponding SAXS images (Figure 1c) show meridional maxima, indicating that the melt consists of some oriented structures (crystalline or mesomorphic) of higher density than the surrounding amorphous matrix of lower density. Thus, variation in the intensity along the azimuthal angle is expected, which leads to a nonzero f value. Figures 12 and 13 show the increases in f with shear rate and with shear duration, respectively. It is interesting to see that the f value (or the degree of crystal orientation) appears to approach a plateau value at a high shear rate or a high shear duration. These results are consistent with the corresponding SAXS results discussed earlier. Our interpretations of these interesting results are presented in the following section, along with results of the oriented crystal fraction obtained from the rheo-SAXS/WAXD data.

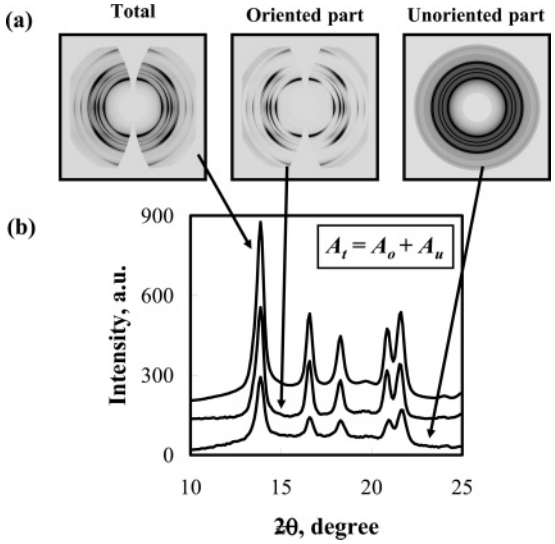

Figure 14. (a) Fraser-corrected WAXD (total) pattern of a sheared iPP sample at room temperature (shear rate 45 s^{-1} and shear duration 5 s) and the corresponding oriented and unoriented patterns obtained after deconvolution by the halo method.[83] (b) Circularly averaged WAXD intensity profiles extracted from the total, oriented, and unoriented patterns in (a).

(e) Oriented Crystal Fraction in Sheared iPP Samples at Room Temperature. The fraction of oriented crystals in the sheared iPP sample cooled to room temperature was determined by the "halo" method.[83] The principle of this method is as follows: The total intensity, scattered or diffracted, I_{total}[**s** or 2θ, ϕ], is equal to the sum of two components: $I_{oriented}$[**s** or 2θ, ϕ] and $I_{unoriented}$[**s** or 2θ]. The scattered or diffracted intensity due to the oriented crystals, $I_{oriented}$[**s** or 2θ, ϕ], is azimuthal dependent, while that due to the unoriented crystals (and amorphous phase), $I_{unoriented}$-[**s** or 2θ], is azimuthal independent. The fraction of $I_{unoriented}$[**s** or 2θ] can be estimated by the following procedures. The envelope of minimum scattered or diffracted intensity values is obtained by drawing a series of azimuthal scans along the scattering vector or diffraction angle, and is attributed to the contribution of the unoriented crystals. The difference between I_{total}-[**s** or 2θ, ϕ] and $I_{unoriented}$[**s** or 2θ] is attributed to the contribution of the oriented crystals. The oriented crystal fraction is defined as the ratio of the integrated $I_{oriented}$ and integrated I_{total} values.

The example analysis of the WAXD data using the above method is illustrated in Figure 14a, where the total intensity pattern of the sheared iPP sample (rate 60 s^{-1}, $t_s = 3$ s) at room temperature along with contributions from the unoriented and oriented components are shown. In this figure, the total diffracted intensity was determined from the 2D WAXD pattern after the "Fraser correction".[82] As mentioned earlier this correction was found not to be critical for the estimate of the total crystallinity (X_t). In Figure 14a, A_t, A_o, and A_u represent the area sums of all diffraction peaks in the 2D profile of the total intensity (Fraser corrected), oriented contribution, and unoriented contribution, respectively. The calculated values of the three area sums have the following relationship: $A_t = A_o + A_u$. This relationship was also confirmed by the addition rule of the three circularly averaged intensity profiles (Figure 14b) extracted from their corresponding 2D patterns (Figure 14a). The latter method provided an internal

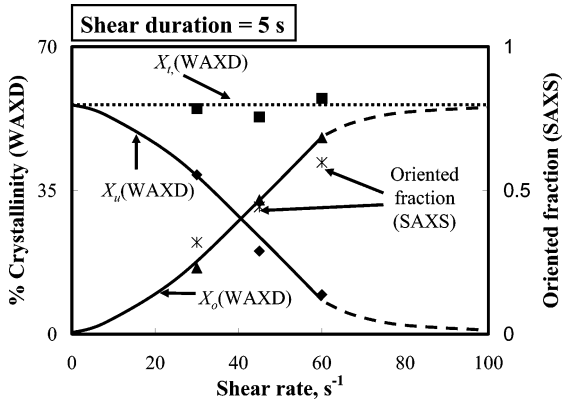

Figure 15. Total crystallinity, crystallinity values due to oriented and unoriented crystals (WAXD), and oriented fraction from SAXS (the data point is indicated with an asterisk) of the fully crystallized polymer at room temperature as a function of shear rate (constant shear duration 5 s).

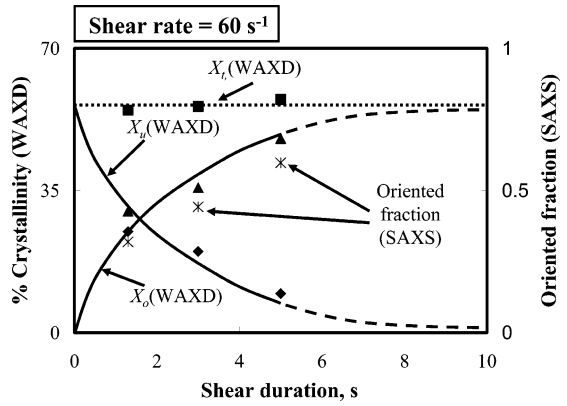

Figure 16. Total crystallinity, crystallinity values due to oriented and unoriented crystals (WAXD), and oriented fraction from SAXS (the data point is indicated with an asterisk) of the fully crystallized polymer at room temperature as a function of shear duration (constant shear rate 60 s^{-1}).

check for the accuracy of the image−image subtraction procedure using the halo method.[83] The percent crystallinity values due to the oriented (X_o) and unoriented (X_u) crystals were obtained from the corresponding area sums as follows:

$$X_t = X_o + X_u \tag{4}$$

$$\frac{X_o}{X_u} = \frac{A_o}{A_u} \tag{5}$$

Figure 15 shows the values of X_t, X_o, and X_u of the fully crystallized sheared iPP sample (t_s = 5 s) at room temperature as a function of shear rate. The oriented fraction in the corresponding SAXS image (Figure 3) was also calculated, and the results are superimposed in Figure 15 (the data point is illustrated as an asterisk). Similarly, the values of these parameters as a function of shear duration are presented in Figure 16. The main features in Figures 15 and 16 can be summarized as follows. (1) The total crystallinity (53−57%) is about constant under all shear conditions. (2) The crystallinity due to oriented crystals (from WAXD) increases with both shear rate and shear duration; conversely, the crystallinity due to unoriented crystals decreases. (3) The oriented fraction, extracted by analyzing the SAXS data using a deconvolution method similar to that demonstrated above, increases with both shear rate and shear duration, showing a trend similar to that of the WAXD results. (4) The crystallinity due to oriented crystals appears to reach a plateau value at a high shear rate as well as at a high shear duration. Theoretically, the upper limit for the plateau value is the total crystallinity, which is not likely to be achieved in practice. As the fraction of oriented crystals formed at room temperature is indicative of molecular orientation/extension achieved at high temperature, it is our opinion that there is a certain limiting value for molecular orientation/extension even at intense shear field conditions. Our interpretations of this important observation are presented in the Discussion.

It should be noted that the oriented fraction extracted from SAXS and the value of X_o/X_t from WAXD do not represent the same quantity. The value from WAXD is much higher than the oriented fraction value calculated from SAXS. This can be explained as follows. In WAXD, the intensity of the crystal diffraction peaks is significantly stronger than the intensity of the amorphous background. Therefore, the contributions of amorphous and crystalline phases can be accurately determined from the peak-fit procedure. On the other hand, the SAXS intensity is proportional to the electron density difference between the scatterer and the surrounding matrix. Therefore, the SAXS intensity due to the amorphous phase contribution alone is extremely small because it possesses almost no density contrast, and cannot be separated from the total SAXS intensity. Thus, the oriented fraction from SAXS is lower than that from WAXD. Nevertheless, the observed trend in the calculated fraction value from SAXS as a function of the shear intensity is consistent with the corresponding WAXD results. This result suggests that the bulk of the residual orientation in these sheared samples may be due to amorphous rather than crystalline orientation.

Discussion

In situ rheo-SAXS and -WAXD results clearly show that the shear flow intensity (rate and duration) significantly affects the crystallization precursor structure in the polymer melt and the final morphology in the resulting solid. These results provide a microscopic insight into several important aspects of the molecular organization in the polymer melt under shear and how it affects the microstructure and morphology of the crystallized polymer. A summary of important findings is presented below.

Characteristics of Shear-Induced Shish-Kebab in iPP. It is well-known that when a semicrystalline polymer melt is subjected to shear or elongational flow, a shish-kebab structure can be devloped in the polymer matrix. The typical pathway toward the formation of shish-kebab morphology is as follows: The applied flow field, such as shear in this study, causes orientation of polymer chain segments in the flow direction. It is generally thought that the oriented chain segments can organize into a parallel array and form a precursor of primary nuceli. When the cluster of chain segments is above a certain critical size, it forms a stable nucleus. Although this is a very fast process, which is dictated by stochastic events such as Brownian motion of chain segments, the relaxation of chain orientation clearly has a significant effect on the formation of stable primary nuclei. Under intense shear conditions, such as those used in our experiments, high orientation/extension of chains along the flow direction promotes a linear as-

sembly of multiple nuclei (the assembly is thus termed a shish). In SAXS experiments, the uncorrelated shish structures cause equatorial streaks. Figures 1 and 2 show the emergence of equatorial steaks immediately after shear, which is direct evidence of the shish formation in the melt. Primary nuclei in the shish provide nucleation sites for the attachment of folded-chain crystals, which grow laterally through the process of secondary crystallization and form stacks of lamellae (they are termed kebabs). Scattering maxima along the meridian in the SAXS patterns of Figures 1−3 are evidence of the formation of kebabs in the melt.

While there are numerous examples in the literature about the observation of shish-kebab structure in flow, the characteristics of the shish-kebab structure were rarely determined. Advanced imaging techniques, such as atomic force microscopy (AFM), are now available and have proven to be useful for viewing the fine microstructure of shish-kebab structures in real space. For example, a recent publication by Hobbs et al.[84] shows images of the shish-kebab structure in a sheared polyethylene melt. From these images, the estimated shish length can be up to several micrometers. Our results in Figures 8 and 9 give a quantitative estimate of the average sizes of the shish-kebab structure (the average shish length was 700−750 nm, and the average long period in the kebabs was 60−70 nm) in the sheared iPP melt within the X-ray irradiation volume. We expect that there was a wide distribution of the shish-kebab length because of the variation of the strain along the thickness direction in the parallel-plate rheometer (the strain was high near the rotating plate and 0 near the stationary plate). It is conceivable that the long shish could be over several micrometers in length.

Shear Rate versus Shear Duration. The macroscopic strain is the product of shear rate and shear duration. Either parameter can be varied to achieve the same bulk strain. Consider the molecular orientation/extension in the following two flow conditions: (a) long-duration shear at a *very low rate* and (b) *very-short-duration* shear at a high rate; here *very low* or *very short* means appraching zero. In (a) at a *very low rate*, only small degrees of orientation and extension of chain segments can be realized; in (b) with *very-short-duration* shear, the oriented chain segments can remain oriented only for a short time, which may not be long enough for the formation of a stable nucleus. Thus, the probability of the formation of stable nuclei is small in both cases. Hence, a certain minimum critical shear rate as well as shear duration is required to significantly affect the molecular orientation and resultant microstructure.

The qualitative and quantitative effects of the imposed flow condition, (1) varying shear rate at a constant shear duration and (2) varying shear duration at a constant shear rate, are discussed below. Let us compare results under the following flow conditions: (I) (A1) shear rate 60 s^{-1}, $t_s = 1.3$ s (strain 78) versus (B1) shear rate 30 s^{-1}, $t_s = 5$ s (strain 150); (II) (A2) shear rate 60 s^{-1}, $t_s = 3$ s (strain 180) versus (B2) shear rate 45 s^{-1}, $t_s = 5$ s (strain 225). SAXS patterns in Figures 1 and 2 clearly show, qualitatively, that the SAXS intensity at flow conditions A1 and A2 is stronger than that in B1 and B2, respectively. In addition, the corresponding WAXD patterns in Figures 4 and 5 show a trend similar to that above. Quantitatively, Figure 11 shows that the total crystallinity, X_t, at A1 and A2 is higher than that at B1 and B2, respectively. Also, Figures 12 and 13 show

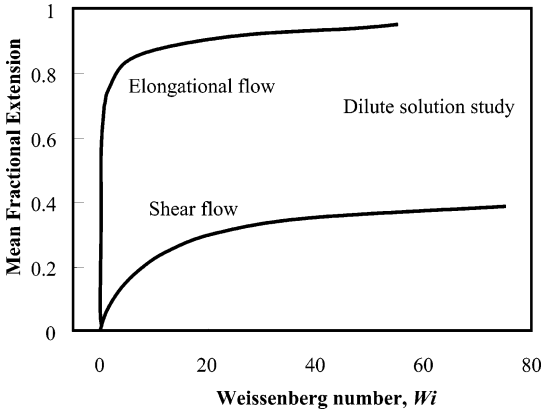

Figure 17. Mean fractional extension of molecules versus the Weissenberg number, *Wi*, in shear and elongational flow.[65]

that the orientation function, *f*, at A1 and A2 is higher than that at B1 and B2, respectively. These results are clear evidence of a higher degree of molecular orientation at A1 and A2 compared to B1 and B2. The final polymer microstructure characterized by the fraction value of oriented crystals in a fully crystallized polymer also confirmed the above conclusion. It is evident from the SAXS intensity in Figure 3 and the WAXD intensity in Figures 6 and 7 that the amount of oriented crystals at A1 and A2 is higher than that at B1 and B2, respectively. The percent crystallinity due to the oriented crystals determined by WAXD and the oriented fraction in SAXS (Figures 15 and 16) also support the above interpretations. Clearly, the degree of crystal orientation and amount of oriented crystals are higher in short-duration shear at a high shear rate than those in long-duration shear at a low shear rate. Thus, we conclude that, at a constant strain, molecular orientation/extension can be induced more effectively in short-duration shear at a high shear rate than that in long-duration shear at a low shear rate.

Weissenberg Number and Molecular Orientation. The degree of polymer orientation/extension is, obviously, dependent on its characteristic properties: viscosity, chain reptation, relaxation behavior, etc. In general, the polymer chain in flow begins to deform when the force due to hydrodynamic friction across the chain exceeds the entropic elasticity of the coiled chain. There are two natural time scales. The first time scale is the longest relaxation time of the polymer chain (λ_{max}), which is the characteristic time that is necessary for Brownian motion to globally rearrange the chain conformation. The second time scale is set by the inverse strain rate of the applied flow (i.e., the reciprocal of the elongational or shear rate). Dimensionless parameters, the Deborah number in elongational flow ($De = \lambda_{max} \times$ elongational rate) or Weissenberg number in shear flow ($Wi = \lambda_{max} \times$ shear rate) can be used to characterize the strength of the applied flow field. Figure 17 shows the behavior of a single polymer molecule in dilute solution proposed by Chu et al.[65] It is seen that in shear the mean fractional extension increases gradually with *Wi* and approaches an asymptotic value at high values of *Wi*, while in pure elongational flow, the extension rises very rapidly to a value close to the full contour length of the chain at relatively low *Wi* values. Although the situation in the polymer melt under shear is not clear, one might hypothesize that the behavior of the mean fractional extension versus *Wi* might be, qualitatively, similar to that in dilute solution. This is

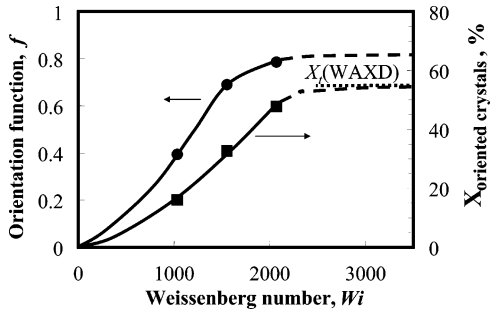

Figure 18. Herman's orientation function, f (as shown by filled circles), of the sheared melt (at 165 °C and 1 h after shear) and the crystallinity due to oriented crystals, X_o (as shown by filled squares) of the crystallized polymer at room temperature as a function of the Weissenberg number, Wi.

because the degree of crystal orientation and the amount of oriented crystals are, undoubtedly, related to the extent of molecular orientation/extension in the melt. Results of the present studies are extended to gain insight into the molecular mechanisms in an entangled melt under shear.

In our shear experiments, we measured three flow parameters: shear rate, shear duration, and temperature. All experiments were performed at a constant temperature of 165 °C. Hence, in constant shear-duration experiments, the Weissenberg number can be directly related to the shear rate. The longest relaxation time at an experimental temperature of 165 °C was estimated from the rheological data of dynamic moduli, $G'(\omega)$ and $G''(\omega)$, measured in small-amplitude oscillatory shear experiments at several temperatures. Horizontal temperaure shift factors, a_T, were calculated from the dynamic moduli data. The discrete relaxation time spectrum was determined by a nonlinear regression fit of the G' and G'' master curves at a reference temperature of 140 °C. The estimated value of the longest relaxation time, λ_{max} (= 70 s), was the time when the relaxation strength dropped by more than 2 orders of magnitude. The λ_{max} at other temperatures was calculated from the horizontal shift factors. The estimated value of λ_{max} at 165 °C was 34.5 s.

Figure 18 shows f and X_o versus Wi, where f is Herman's orientation function of the (110) reflection at high temperature (Figure 12) and X_o is the percent crystallinity due to oriented crystals in the fully crystallized sample at room temperature (Figure 15). The orientation function represents the average degree of crystal orientation in the sheared iPP melt at 165 °C and is related to the mean orientation/extension of the polymer molecules in flow. The subsequent cooling of the sheared melt allows all crystallizable species to crystallize. As the surface of already formed oriented crystals can act as nuclei for the crystallizing species, the melt that has a greater number of nuclei will result in a greater amount of the oriented crystals (X_o) in the fully crystallized polymer. In Figure 18, both f and X_o appear to reach plateau values at high Wi, showing a very similar trend. Although the exact magnitude of the mean extension of molecules cannot be determined, we expect that it will vary with Wi in a similarly to f and X_o with Wi. In other words, we predict that, in an entangled polymer melt, the mean molecular extension gradually increases with Wi and reaches a plateau value at high values of Wi, similar to the obervations in dilute polymer solutions. The magnitude of the plateau value of the mean molecular extension in shear is probably significantly lower than the value in elongational flow. This is so for the following reason:[65] The pure elongational flow has no rotational components and can drastically stretch polymer chains even at low flow strengths. Hence, an abrupt *coil−stretch* transition for polymers in extensional flow is expected[85] and has been observed in experiments with polymer solutions.[63−67] Shear flow has both extensional and rotational components. The extensional component orients and/or stretches polymer molecules; the rotational component causes end-over-end tumbling, and the stretched state is destabilized. Thus, molecules stretch, tumble, and retract in a stochastic manner. Since both the stretching and tumbling components are driven by the velocity gradient, the random stretching and contraction process occurs more frequently at higher shear rates, which was experimentally observed in the dilute solution studies.[65] Thus, in an entangled melt, the mean molecular orientation/extension that can be achieved in shear should be much lower than the full contour length even at high values of Wi.

Conclusions

(1) In an iPP melt under shear flow, both the degree of crystal orientation (f) at 165 °C and the fraction of oriented crystals (X_o) in a fully crystallized sample at room temperature were found to increase with shear rate (at a constant shear duration) as well as with shear duration (at a constant shear rate). The value of f is directly related to the extent of molecular orientation/extension in the melt induced by shear, and also affects the magnitude of X_o that can be obtained in the final solid state.

(2) Careful examination of rheo-SAXS and -WAXD data indicated that, at a constant strain, short-duration shear at a high shear rate is more effective in enhancing the molecular orientation and subsequent crystallization (higher f and X_o) than long-duration shear at a low shear rate.

(3) Both f and X_o increase gradually with the Weissenberg number, Wi, and reach plateau values at high Wi values. There appears to be a limiting value for the mean extension of molecules in an entangled polymer melt under shear; it is much lower than the full contour length even at high Wi values.

(4) The average characteristic lengths of the shish-kebab entity in a sheared iPP melt were estimated from the rheo-SAXS data. It was found that the average shish length, under the chosen experimental conditions, was 700−750 nm long and the average long period between the adjacent lamellae in the kebabs was 60−70 nm.

Acknowledgment. We acknowledge the assistance of Drs. Igors Sics and Carlos Avila-Orta for synchrotron SAXS and WAXD experimental setup. The financial support of this work was provided by the NSF (Grant DMR-0405432) and the ExxonMobil Chemical Co.

References and Notes

(1) Wunderlich, B. *Macromolecular Physics*; Academic: New York, 1973; Vol. 2.
(2) Pennings, A. J.; Van der mark, J. M. A.; Booij, H. C. *Kolloid Z. Z. Polym.* **1970**, *236*, 99.
(3) Pennings, A. J.; Kiel, A. M. *Kolloid Z. Z. Polym.* **1965**, *205*, 160.
(4) Lieberwirth, I.; Loos, J.; Petermann, J.; Keller, A. *J. Polym. Sci., Part B: Polym. Phys.* **2000**, *38*, 1183.
(5) Petermann, J.; Miles, M.; Gleiter, H. *J. Polym. Sci., Part B: Polym. Phys.* **1979**, *17*, 55.

(6) White, H. M.; Bassett, D. C. *Polymer* **1997**, *38* (22), 5515.
(7) Varga, J. *J. Mater. Sci.* **1992**, *27*, 2557.
(8) Varga, J.; Karger-Kocsis, J. *J. Polym. Sci., Part B: Polym. Phys.* **1996**, *34* (4), 657.
(9) Vleeshouwers, S.; Meijer, H. E. H. *Rheol. Acta* **1996**, *35*, 391.
(10) Goschel, U.; Swartjes, F. H. M.; Peters, G.. W. M.; Meijer, H. E. H. *Polymer* **2000**, *41* (4), 1541.
(11) Bove, L.; Nobile, M. R. *Macromol. Symp.* **2002**, *185*, 135.
(12) Kitoko, V.; Keentok, M.; Tanner, R. I. *Korea-Aust. Rheol. J.* **2003**, *15* (2), 63.
(13) Lellinger, D.; Floudas, G.; Alig, I. *Polymer* **2003**, *44*, 5759.
(14) Watanabe, K.; Suzuki, T.; Masubuchi, Y.; Taniguchi, T.; Takimoto, J.; Koyama, K. *Polymer* **2003**, *44*, 5843.
(15) Ran, S.; Wang, Z.; Burger, C.; Chu, B.; Hsiao, B. S. *Macromolecules* **2002**, *35*, 10102.
(16) Coppola, S.; Grizzuti, N.; Maffettone, P. L. *Macromolecules* **2001**, *34*, 5030.
(17) Gee, R. H.; Fried, L. E. *J. Chem. Phys.* **2003**, *118*, 3827.
(18) Keller, A.; Kolnaar, H. W. *Mater. Sci. Technol*. **1997**, *18*, 189.
(19) Keller, A.; Hikosaka, M.; Rastogi, S. *Phys. Sci.* **1996**, *T66*, 243.
(20) Keller, A.; Hikosaka, M.; Rastogi, S.; Toda, A.; Barham, P. J.; Goldbeck-Wood, G.. *J. Mater. Sci.* **1994**, *29*, 2579.
(21) Keller, A.; Cheng, S. Z. D. *Polymer* **1998**, *39*, 4461.
(22) Mackley, M. R.; Keller, A. *Polymer* **1973**, *14*, 16.
(23) Pope, D. P.; Keller, A. *Colloid Polym. Sci.* **1978**, *256*, 751.
(24) Miles, M. J.; Keller, A. *Polymer* **1980**, *21*, 1295.
(25) Eder, G.; Janeschitz-Kriegl, H. *Mater. Sci. Technol*. **1997**, *18*, 268.
(26) Jerschow, P.; Janeschitz-Kriegl, H. *Int. Polym. Process.* **1997**, *12* (1), 72.
(27) Eder, G.; Janeschitz-Kriegl, H.; Liedauer, S. *Prog. Polym. Sci.* **1990**, *15*, 629.
(28) Liedauer, S.; Eder, G.; Janeschitz-Kriegl, H.; Jerschow, P.; Geymayer, W.; Ingolic, E. *Int. Polym. Process.* **1993**, *8* (3), 236.
(29) Pogodina, N. V.; Lavrenko, V. P.; Winter, H. H.; Srinivas, S. *Polymer* **2001**, *42*, 9031.
(30) Pogodina, N. V.; Siddiquee, S. K.; Egmond, J. W.; Winter, H. H. *Macromolecules* **1999**, *32*, 1167.
(31) Pogodina, N. V.; Winter, H. H.; Srinivas, S. *J. Polym. Sci., Part B: Polym. Phys.* **1999**, *37* (24), 3512.
(32) Pogodina, N. V.; Winter, H. H. *Macromolecules* **1998**, *31* (23), 8164.
(33) Kumaraswamy, G.; Kornfield, J. A.; Yeh, F.; Hsiao, B. S. *Macromolecules* **2002**, *35*, 1762.
(34) Seki, M.; Thurman, D. W.; Oberhauser, J. P.; Kornfield, J. A. *Macromolecules* **2002**, *35*, 2583.
(35) Kumaraswamy, G.; Verma, R. K.; Wang, P.; Kornfield, J. A.; Yeh, F.; Hsiao, B. S.; Olley, R. H. *Polymer* **2000**, *41* (25), 8931.
(36) Kumaraswamy, G.; Issaian, A. M.; Kornfield, J. A. *Macromolecules* **1999**, *32* (22), 7537.
(37) Strobl, G. *Eur. Polym. J.* **2000**, *E3*, 165.
(38) Iijima, M.; Strobl, G. *Macromolecules* **2000**, *33*, 5204.
(39) Fu, Q.; Heck, B.; Strobl, G.; Thomann, Y. *Macromolecules* **2001**, *34*, 2502.
(40) Lotz, B. *Eur. Polym. J.* **2000**, *E3*, 185.
(41) Fillon, B.; Thierry, A.; Wittmann, J. C.; Lotz, B. *J. Polym. Sci., Part B: Polym. Phys.* **1996**, *31* (10), 1407.
(42) Mathieu, C.; Thierry, A.; Wittmann, J. C.; Lotz, B. *Polymer* **2000**, *41*, 7241.
(43) Mitchell, G. R.; Holt, J. J.; Thornley, S. A.; Chai, C. K. *Proceedings of the International Conference on Flow Induced Crystallization of Polymers*, Salerno, Italy, Oct 14−17, 2001; p 15.
(44) Pople, J. A.; Mitchell, G. R.; Sutton, S. J.; Vaughan, A. S.; Chai, C. K. *Polymer* **1999**, *40*, 2769.
(45) Li, L.; Jeu, W. H. *Phys. Rev. Lett.* **2004**, *92*, 075506.
(46) Li, L.; Jeu, W. H. *Macromolecules* **2003**, *36*, 4862.
(47) Duplay, C.; Monasse, B.; Haudin, J.; Costa, J. *Polym. Int.* **1999**, *48*, 320.
(48) Devaux, N.; Monasse, B.; Haudin, J. M.; Vermant, J.; Moldenaers, P.; Andre, J. M.; Ernst, B. *Proceedings of the International Conference on Flow Induced Crystallization of Polymers*, Salerno, Italy, 14−17, 2001; p 31.
(49) Haudin, J.; Duplay, C.; Monasse, B.; Costa, J. L. *Macromol. Symp.* **2002**, *185*, 119.
(50) Ryan, A. J.; Terrill, N. J.; Fairclough, J. P. A. In *Scattering of Polymers*; Cebe, P., Hsiao, B. S., Lohse, D. J., Eds.; ACS Symposium Seriers 739; American Chemical Society: Washington, DC, 2000; p 201.
(51) Terrill N. J.; Fairclough, J. P. A.; Towns-Andrews, E.; Komanschek, B. U.; Young, R. J.; Ryan, A. J. *Polymer* **1998**, *39* (11), 2381.
(52) Ryan, A. J.; Stanford, J. L.; Bras, W.; Nye, T. M. W. *Polymer* **1997**, *38* (4), 759.
(53) Wilkinson, A. N.; Ryan, A. J. *Polymer processing and Structure Development*; Kluwer: Dodrecht, The Netherlands, 1998.
(54) Liu, C.; Muthukumar, M. *J. Chem. Phys.* **1998**, *109*, 2536.
(55) Muthukumar, M. *Eur. Phys. J. E: Soft Matter* **2000**, *3* (2), 199.
(56) Muthukumar, M.; Welch, P. *Polymer* **2000**, *41*, 8833.
(57) Dukovski, I.; Muthukumar, M. *J. Chem. Phys.* **2003**, *118*, 6648.
(58) Alfonso, G. C.; Azzurri, F. *Proceedings of the International Conference on Flow Induced Crystallization of Polymers*, Salerno, Italy, Oct 14−17, 2001; p 27.
(59) Alfonso, G. C.; Ziabicki, A. *Colloid Polym. Sci.* **1995**, *273*, 317.
(60) Ziabicki, A.; Alfonso, G. C. *Macromol. Symp*. **2002**, *185*, 211.
(61) Garcia Gutierrez, M.-C.; Alfonso, G. C.; Riekel, C.; Azzurri, F. *Macromolecules* **2004**, *37*, 478.
(62) Hu, W.; Frenkel, D.; Mathot, V. B. F. *Macromolecules* **2003**, *36*, 8178.
(63) Perkins, T. T.; Smith, D. E.; Chu, S. *Science* **1997**, *276*, 2016.
(64) Smith, D. E.; Babcock, H. P.; Chu, S. *Science* **1998**, *281*, 1335.
(65) Smith, D. E.; Babcock, H. P.; Chu, S. *Science* **1999**, *283*, 1724.
(66) Schroeder, C. M.; Babcock, H. P.; Shaqfeh, E. S. G.; Chu, S. *Science* **2003**, *301*, 1515.
(67) Babcock, H. P.; Teixeira, R. E.; Hur, J. S.; Shaqfeh, E. S. G.; Chu, S. *Macromolecules* **2003**, *36*, 4544.
(68) Wang, Z. G.; Hsiao, B. S.; Sirota, E.; Agarwal, P.; Srinivas, S. *Macromolecules* **2000**, *33*, 978.
(69) Somani, R. H., Yang, L.; Hsiao, B. S.; Agarwal, P.; Fruitwala, H.; Tsou, A. H. *Macromolecules* **2002**, *35*, 9096.
(70) Somani, R. H.; Yang, L.; Hsiao, B. S. *Physica A* **2002**, *304*, 145.
(71) Somani, R. H.; Nogales, A.; Srinivas, S.; Fruitwala, H.; Tsou, A. H.; Hsiao, B. S. *Proceedings of the International Conference on Flow Induced Crystallization of Polymers*, Salerno, Italy, Oct 14−17, 2001; p 21.
(72) Somani, R. H.; Bruger, C.; Hsiao, B. S.; Stein, R. S. *Proceedings of ACS Division of Polymeric Materials: Science and Engineering*, Chicago, Aug 26−30, 2001; American Chemical Society: Washington, DC, Vol. 85, p 429.
(73) Somani, R. H.; Hsiao, B. S.; Nogales, A.; Srinivas, S. Tsou, A. H.; Sics, I.; Balta-Calleja, F.; Ezquerra, T. A. *Macromolecules* **2000**, *33*, 9385.
(74) Nogales, A.; Hsiao, B. S.; Somani, R. H.; Srinivas, S. Tsou, A. H.; Balta-Calleja, F.; Ezquerra, T. A. *Polymer* **2000**, *42*, 5247.
(75) Somani, R. H.; Hsiao, B. S.; Nogales, A.; Srinivas, S. Tsou, A. H.; Balta-Calleja, F.; Ezquerra, T. A. *Macromolecules* **2001**, *34*, 5902.
(76) Agarwal, P. K.; Somani, R. H.; Weng, W.; Mehta, A.; Yang, L.; Ran, S.; Liu, L.; Hsiao, B. S. *Macromolecules* **2003**, *36*, 5226.
(77) Somani, R. H., Yang, L.; Hsiao, B. S.; Fruitwala, H. *J. Macromol. Sci., Part B* **2003**, *B42*, 515.
(78) Yang, L.; Somani, R. H.; Sics, I.; Hsiao, , B. S.; Kolb, R.; Lohse, D.; Fruitwala, H. *Macromolecules* **2004**, *37* (13), 4845−4859.
(79) Ran, S.; Zong, X.; Fang, D.; Hsiao, B. S.; Chu, B.; Phillips, R. A. *Macromolecules* **2001**, *34* (8), 2569.
(80) Ruland, W. *J. Polym. Sci., Part C* **1969**, *28*, 143.
(81) Fraser, R. D. B.; Macrae, T. P.; Miller, A.; Rowlands, R. J. *J. Appl. Crystallogr.* **1976**, *9*, 81.
(82) Alexander, L. E. *X-ray Diffraction in Polymer Science*; Wiley: New York, 1969.
(83) Ran, S.; Zong, X.; Fang, D.; Hsiao, B. S.; Chu, B.; Ross, R. *J. Appl. Crystallogr.* **2000**, *33*, 1031.
(84) Hobbs, J. K.; Miles, M. J. *Macromolecules* **2001**, *34*, 353.
(85) de Gennes, P. G. *J. Chem. Phys.* **1974**, *60*, 5030.

MA048285D